Metformin induces muscle atrophy by transcriptional regulation of myostatin via HDAC6 and FoxO3a

Min Ju Kang, Ji Wook Moon, Jung Ok Lee, Ji Hae Kim, Eun Jeong Jung, Su Jin Kim, Joo Yeon Oh, Sang Woo Wu, Pu Reum Lee, Sun Hwa Park & Hyeon Soo Kim*

Department of Anatomy, Korea University College of Medicine, Seoul, Republic of Korea

Abstract

Background   Skeletal muscle atrophy is a severe condition that involves loss of muscle mass and quality. Drug intake can also cause muscle atrophy. Biguanide metformin is the first-line and most widely prescribed anti-diabetic drug for patients with type 2 diabetes. The molecular mechanism of metformin in muscle is unclear.
Methods   Myostatin expression was investigated at the protein and transcript levels after metformin administration. To investigate the pathways associated with myostatin signalling, we used real-time polymerase chain reaction, immunoblotting, luciferase assay, chromatin immunoprecipitation assay, co-immunoprecipitation, immunofluorescence, primary culture, and confocal microscopy. Serum analysis, physical performance, and immunohistochemistry were performed using our *in vivo* model.
Results   Metformin induced the expression of myostatin, a key molecule that regulates muscle volume and triggers the phosphorylation of AMPK. AMPK alpha2 knockdown in the background of metformin treatment reduced the myostatin expression of C2C12 myotubes ($-49.86 \pm 12.03\%$, $P < 0.01$) and resulted in increased myotube diameter compared with metformin ($+46.62 \pm 0.88\%$, $P < 0.001$). Metformin induced the interaction between AMPK and FoxO3a, a key transcription factor of myostatin. Metformin also altered the histone deacetylase activity in muscle cells (>3.12-fold ± 0.13, $P < 0.001$). The interaction between HDAC6 and FoxO3a induced after metformin treatment. Confocal microscopy revealed that metformin increased the nuclear localization of FoxO3a (>3.3-fold, $P < 0.001$). Chromatin immunoprecipitation revealed that metformin induced the binding of FoxO3a to the myostatin promoter. The transcript-level expression of myostatin was higher in the gastrocnemius (GC) muscles of metformin-treated wild-type (WT) ($+68.9 \pm 10.01\%$, $P < 0.001$) and db/db mice ($+55.84 \pm 6.62\%$, $P < 0.001$) than that in the GC of controls ($n = 4$ per group). Average fibre cross-sectional area data also showed that the metformin-treated C57BL/6J (WT) ($-31.74 \pm 0.75\%$, $P < 0.001$) and C57BLKS/J-db/db ($-18.11 \pm 0.94\%$, $P < 0.001$) mice had decreased fibre size of GC compared to the controls. The serum myoglobin level was significantly decreased in metformin-treated WT mice ($-66.6 \pm 9.03\%$, $P < 0.01$).
Conclusions   Our results demonstrate that metformin treatment impairs muscle function through the regulation of myostatin in skeletal muscle cells via AMPK-FoxO3a-HDAC6 axis. The muscle-wasting effect of metformin is more evident in WT than in db/db mice, indicating that more complicated mechanisms may be involved in metformin-mediated muscular dysfunction.

Keywords   Myostatin; AMPK; FoxO3a; HDAC6; Muscle atrophy; Metformin

Introduction

Skeletal muscle atrophy, a remarkable loss of muscle, is characterized by a decrease in muscle fibre size and protein content[1] and occurs when protein degradation rates exceed the rate of protein synthesis. Skeletal muscle atrophy is reportedly associated with inactivity, ageing, and various diseases and can occur as a side effect of some drugs.[2,3]

One mechanism that regulates muscle mass and strength is signalling by myostatin, one of the master regulators of skeletal muscle growth. Myostatin plays a central role in the development and maintenance of skeletal muscle by acting as a negative regulator of muscle mass.[4–6] It predominantly produced in the skeletal muscle, and a decrease in the gene expression or activity of myostatin results in increased muscle mass and hypertrophy.[7,8] Increased myostatin expression has been observed in different disease states, including type 2 diabetes mellitus (T2DM) and cancer. In particular, patients with T2DM experience a loss of muscle mass and quality. Insulin resistance and high blood glucose levels accelerate this condition, and patients with these conditions exhibit increased serum myostatin levels.[9–11]

Metformin is an AMPK agonist that is commonly administered therapeutically to patients with T2DM to decrease hepatic glucose production and intestinal absorption of glucose. Metformin also improves insulin sensitivity by increasing peripheral glucose uptake and utilization. AMPK inhibits anabolic processes such as protein synthesis, enhances protein degradation and autophagy, and[12,13] decreases serum glucose levels.[14,15] Metformin administration ameliorates diabetes by affecting glucose absorption, but long-term metformin administration is associated with side effects, such as muscle atrophy. Metformin administration might induce muscle atrophy.[16–18] The mechanisms of action of metformin are unknown, but metformin up-regulates the expression of atrophy-related genes, MuRF1 and MAFbx32, and enhance the activity of ubiquitin proteasome system.[19] However, the specific mechanisms underlying these phenomena are poorly understood. In this study, we report that metformin might induce muscle atrophy by inducing the nuclear import of FoxO3a and that this phenomenon is regulated in an AMPK-dependent manner. Our results reveal a novel AMPK-FoxO3a-HDAC6 axis that underlies muscle atrophy.

Materials and methods

Cell culture

C2C12 myoblasts were maintained in the proliferation medium comprising Dulbecco's modified Eagle's medium (DMEM) supplemented with 10% foetal bovine serum (Gibco) and 1% penicillin and streptomycin (WELGENE) at 37°C in a humidified incubator with an atmosphere of 5% CO_2. Human skeletal myoblasts were maintained in the proliferation medium comprising DMEM supplemented with 2% horse serum (Gibco) and 1% penicillin and streptomycin (WELGENE) at 37°C in a humidified incubator with an atmosphere of 5% CO_2.

Animals

Animal experiments were approved by the Korea University Institutional Animal Care and Use Committee and were performed in accordance with the relevant guidelines and regulations. Male C57BLKS/J-db/db and C57BL/6J mice were obtained from Japan SLC (Hamamatsu, Japan) at 6 weeks of age and housed in a highly controlled environment (temperature, 21–23°C; relative moisture, 50–60%; 12 h light:12 h dark cycle). The mice had ad libitum access to water and a standard chow diet. The animals were randomly divided into four groups (*n* = 10 per group), and the experiments were conducted when the mice were 7 weeks old (after acclimation). The mice received either an IP injection of metformin (250 mg/kg) or saline (vehicle) three times a week for 4 weeks. Blood was collected, and the hindlimb muscles were excised for analysis under isoflurane anaesthesia. Hindlimb muscle tissues were resected widely and washed with phosphate-buffered saline (PBS).

Culturing of primary myoblasts

Three-month-old and 23-month-old mice were euthanized to obtain the tibialis anterior (TA) muscle tissue. Tissue was minced to a slurry in a tissue culture plate using razor blades for ~3 min and collagenase and dispase solution, following which 3 mL PBS was added. After triturating by gently pipetting with a 10 ml pipette, the mixture was incubated at 37°C until it became a fine slurry. We then filtered the slurry through a nylon mesh (Cell Strainer, REF352360, BD Falcon). Cells were obtained by centrifuging the slurry at 172 *g* for 5 min and removing the supernatant. The cell pellet was resuspended in 10 mL of F-10-based primary myoblast growth medium and then transferred to a normal culture dish for pre-plating. Then, the suspension was transferred to a collagen-coated dish and incubated. The medium was replaced every 1 or 2 days with fresh F-10-based growth medium. To differentiate myoblasts, the medium was replaced with one containing 2% horse serum in a test plate containing 50–70% confluent cells.

Real-time PCR

Total RNA was extracted from freeze-dried gastrocnemius (GC) muscles and C2C12 myotubes using QIAzol (Qiagen). Thereafter, the RNA concentration was measured using a

Nanodrop spectrophotometer (Thermo Fisher Scientific). cDNA was synthesized using the reverse transcription system (Promega). mRNA expression was assessed by real-time PCR (qRT-PCR) (QuantStudio 3 Real-Time PCR, Thermo Fisher Scientific) using a SYBR Green system (TOPreal™ qPCR 2X Pre-MIX, Enzynomics). The following primers were used: Myostatin forward (5ı-GCA CTG GTA TTT GGC AGA GT-3ı), Myostatin reverse (5ı-TTC AGC CCA TCT TCT CCT GG-3ı), GAPDH forward (5ı-GTG TTC CTA CCC CCA ATG TG-3ı), GAPDH reverse (5ı- CCT GCT TCA CCA CCT TCT TG-3ı), MuRF1 forward (5ı-GTC CAT GTC TGG AGG TCG TT-3ı), MuRF1 reverse (5ı-AGG AGC AAG TAG GCA CCT CA-3ı), MAFbx forward (5ı-ATG CAC ACT GGT GCA AAG AG-3ı), MAFbx reverse (5ı-TGT AAG CAC ACA GGC AGG TC-3ı), FoxO3a forward (5ı-AGC CGT GTA CTG TGG AGC TT-3ı), FoxO3a reverse (5ı-TCT TGG CGG TAT ATG GGA AG-3ı), HDAC6 forward (5ı-AAG TGG AAG AAG CCG TGC TA-3ı), and HDAC6 reverse (5ı-CTC CAG GTG ACA CAT GAT GC-3ı). Data were normalized using GAPDH for each sample, and fold change values were calculated using the ΔΔCt method.

Western blotting

C2C12 myotubes were lysed in a lysis buffer containing protease and phosphatase inhibitors (GenDEPOT). The lysates were loaded onto 10% SDS-PAGE gels and transferred onto 0.45 μm nitrocellulose membranes (GE Healthcare). The membranes were blocked in Tris-buffered saline with Triton X-100 (TBST) containing 0.1% Tween 20 and 5% dry milk (w/v) for 1 h and then washed with TBST. Membranes were incubated overnight with the following primary antibodies: anti-myostatin (GENETEX; GTX32624), anti-p-AMPK(T172) (Cell Signaling; #2535), anti-AMPK α2 (Abcam; ab97275), anti-AMPK α (Cell Signaling; #2532), anti-p-Akt (S473) (Cell Signaling; #4060), anti-Akt (Cell Signaling; #9272), anti-FoxO3a (Cell Signaling; #12829), and anti-HDAC6 (Abcam; ab1440) and then probed with appropriate HRP-conjugated secondary antibodies (Enzo Life Sciences) for 1 h. Chemiluminescence on the blots was visualized using the Amersham Biosciences ECL Detection System (GE Healthcare).

Creatine kinase and lactate dehydrogenase assay

Creatine kinase (CK) activity was determined by the Enzymatic method (Hexokinase) and lactate dehydrogenase (LDH) was determined by the IFCC (International Federation of Clinical Chemistry) standard method using AU480 Chemistry Analyser (Beckman coulter). Both assays were calculated after correction for total protein.

Generation of luciferase reporter plasmids and performance of the luciferase reporter assay

Luciferase reporters for evaluating the activity of the MSTN promoter (1 kb) were constructed using a pGL4.15 vector. The following primers were used: forward (5ı-CGG TAC CTG AGC TCG CTA GCC CTG GAA GCC TGA GTC AAA C-3ı) and reverse (5ı-CTT GAT ATC CTC GAG GCT AGC CAG CAA TCA GCA CAA ACA GG-3ı). PCR products were cloned into the pGL4.15 vectors at Nhe I sites, and the clones were verified by DNA sequencing. C2C12 cells were transiently co-transfected with the myostatin promoter constructs and β-galactosidase reporter plasmids using Lipofectamine 2000 (Invitrogen). The culture medium was replaced with complete medium. After metformin treatment for 12 h, the lysates were analysed for luciferase activity using the Luciferase Assay Reagent (Promega), and luminescence was measured using an EnSpire multimode reader (PerkinElmer). Luciferase activity was normalized to that of β-galactosidase activity.

siRNA transfection

Transfection was performed using Lipofectamine RNAiMax (Invitrogen). For knockdown, siAMPK α2 (Dharmacon, L-040809-00-0010), siFoxO3a (Dharmacon, L-040728-00-0005), siHDAC6 (Dharmacon, L-043456-02-0005), and control siRNA (Santa Cruz, sc-37007) were used. For each experiment, Lipofectamine RNAiMax was diluted with reduced-serum medium (Opti-MEM; Invitrogen) and then mixed with siRNA.

Generation of AMPK α knockout C2C12 cells

To establish AMPK α knockout C2C12 cells, the GeneArt CRISPR Nuclease Vector (Thermo Fisher Scientific) was used according to the manufacturer's instructions, with some modifications. AMPK α knockout was confirmed based on an orange fluorescent protein reporter, which enables the fluorescence-based tracking of the transfection efficiency. C2C12 cells were transfected with the GeneArt CRISPR Nuclease Vector targeting AMPK α using Lipofectamine 2000 (Invitrogen), according to the manufacturer's protocol. Two days post-transfection, AMPK α knockout was confirmed by WB with an anti-AMPK α antibody.

Myogenic differentiation and determination of myotube morphology

C2C12 myoblasts were placed in DMEM containing 2% horse serum (Gibco) and 1% penicillin and streptomycin solution (WELGENE) to induce differentiation. After differentiation,

Lipofectamine (5 μL) mixed with siRNA (100 nM) were treated on C2C12 myotubes for 4 h and replaced with fresh medium. After incubation for 24 h after transfection, metformin was treated for 36 h. Myoblast differentiation was determined by analysing the myotube diameter with haematoxylin and eosin (H&E) staining. Images were captured and processed using a CKX53 microscope (Olympus). All diameters were calculated in 10 random fields from each section using ImageJ software (National Institute of Health).

Immunocytochemistry

For immunofluorescence, cover slips were coated with 0.1% porcine gelatine. Cells were seeded on these cover slips and grown to ~70% confluence. Myoblast differentiation was induced using a differentiation medium. After treatment with or without metformin, cells were fixed in 4% paraformaldehyde (15 min; room temperature) prepared in PBS (137 mM NaCl, 2.68 mM KCl, 1.47 mM KH_2PO_4, and 4.29 mM Na_2HPO_4; pH 7.3). Thereafter, the fixation solution was aspirated, and the cells were washed with PBS. After permeabilization with 0.1% Triton X-100 for 5 min and washing with PBS, the cells were blocked using 1% bovine serum albumin for 30 min. Then, the cells were probed overnight with anti-FoxO3a antibody (#12829; Cell Signaling Technology) or anti-MHC antibody (R&D; MAB4470-SP) prepared in PBS containing 0.1% bovine serum albumin at 4°C. After several washes with PBS containing 0.1% Tween 20, the cells were incubated with Cy3 AffiniPure donkey anti-rabbit IgG (H + L) (red), (Invitrogen; 711-165-152) or Alexa Fluor 488 donkey anti-mouse IgG (H + L) (green) (Invitrogen; A21202) for 45 min at 25°C. Then, the cells were washed with PBS and mounted onto slides using a mounting medium (Biomeda) and observed microscopically using an LSM700 confocal microscope (Carl Zeiss, Göttingen, Germany). The following formula was used to calculate corrected total cell fluorescence (CTCF): CTCF = integrated density − (area of selected cells × mean fluorescence of background readings).

Chromatin immunoprecipitation assay

Chromatin immunoprecipitation (ChIP) assays were performed using an EpiQuik™ acetyl-histone H3 ChIP kit (EPIGENTEK, #P-2010) in accordance with the manufacturer's protocol. Immunoprecipitants were analysed by PCR using the following primer sets: forward (5′-AAC AAA ACA GCA CTC CAA GTC-3′) and reverse (5′-TCG AGG GCA AGC TGA TTC AT-3′) to amplify the FoxO3a-binding site in the MSTN promoter.

Extraction of cytoplasmic and nuclear proteins

NE-PER™ nuclear and cytoplasmic extraction reagents (Thermo Scientific 78833; Rockford, IL, USA) were used to extract cytoplasmic and nuclear proteins. Fractionation was performed according to the manufacturer's instructions. C2C12 myotubes (1×10^6) were mixed with the cytoplasmic extraction reagent I. The cell pellet was gently resuspended and incubated for 10 min on ice. Next, ice-cold cytoplasmic extraction reagent II was added. The tube was vortexed at the highest setting, incubated on ice for 1 min, and then centrifuged at 13 000 rpm for 15 min. The cell supernatant contained the cytoplasmic proteins. To extract the nuclear proteins, the pellet was suspended in NER, vortexed, placed on ice for 40 min, and centrifuged at 13 000 rpm for 10 min. The supernatant (nuclear extract) was immediately transferred into a tube.

Co-immunoprecipitation assay

Cellular proteins (1 mg) were incubated with anti-FoxO3a (rabbit monoclonal antibody) or anti-IgG (normal rabbit antibody) at 4°C for 24 h. Immune complexes were captured with protein A-Sepharose (Amersham, Uppsala, Sweden) after a 3 h incubation. The precipitated immune complexes were washed three times with the wash buffer (25 mM HEPES, 5 mM EDTA, 1% Triton X-100, 50 mM NaF, 150 mM NaCl, 10 mM PMSF). The washed samples were denatured in SDS sample buffer (125 mM Tris–HCl (pH 6.8), 20% (v/v) glycerol, 4% (w/v) SDS, 100 mM DTT, and 0.1% (w/v) bromophenol blue) by boiling at 100°C for 5 min.

In vivo muscle grip strength test

A grip strength test was performed using a calibrated grip strength tester (BIOSEB, BIO-GS3) to assess the grip strength of the fore and hindlimbs (four paws of the mice). The results of the grip strength analysis are represented as means of at least three repetitions.

Histological analysis

Gastrocnemius muscles were fixed with formaldehyde (4%), dehydrated in a graded ethanol series, and cleared in xylene using a Leica AS300S tissue processor (Leica Microsystems). Paraffin-embedded blocks were cut into 4 μm sections using a Leica rotary microtome (RM2255, Leica Microsystems), and the tissues were mounted on slides. Histological examination was performed by H&E staining. The stained sections were scanned using a slide scanner (Axio Scan Z1). To measure the myofibre cross-sectional area, eight non-overlapping

areas of each section were digitally captured, and >250 myofibres were calculated for each sample (n = 4). All muscle fibre areas were calculated using ImageJ (National Institute of Health).

Blood glucose test

The blood glucose test was performed after 12 h of fasting. Blood glucose levels were evaluated via a tail incision in Week 4 of the treatment schedule. Blood glucose was measured using glucose strips that were inserted into an Accu-Check Performa II glucometer (Roche, São Paulo, Brazil). Glycaemic levels were also measured.

Enzyme-linked immunosorbent assay

Enzyme-linked immunosorbent assays (ELISAs) were conducted using a general sandwich-type procedure. Serum myoglobin levels were measured using a sandwich ELISA kit (MBS 564082) in accordance with the manufacturer's protocol.

Statistical analysis

Data are expressed as mean ± standard error of mean. Student's t-test was used to determine the differences between the groups were significant. All statistical analyses were conducted using GraphPad Prism 7 (GraphPad), and significance levels were defined as *$P < 0.05$, **$P < 0.01$, and ***$P < 0.001$.

Results

Metformin up-regulates the expression of myostatin in C2C12 myotubes

To examine the effect of metformin on muscle atrophy, C2C12 myotubes were treated with metformin. Metformin (2 mM) increased the level of mRNA of myostatin, a negative regulator of muscle volume (Figure 1A). Metformin increased the transcript-level expression of myostatin in a time-dependent manner (Figure 1B). Metformin (0.01–2 mM) increased the level of myostatin protein in a dose-dependent and time-dependent manner (Figure 1C and 1D). These results indicate that metformin may induce muscle atrophy in physiological low dose ranges of metformin, as well as high doses of metformin. Metformin is a biguanide. Other biguanides, such as buformin and phenformin, have also been found to increase the level of myostatin protein, suggesting that biguanides might have similar effects on muscle cells (Figure 1E). C2C12 myoblasts were incubated with a differentiation medium until cell fusion and multinucleated myotube formation were achieved. H&E staining and the muscle diameter calculations revealed that metformin (2 mM) significantly reduced the myotube diameter (Figure 1F and 1G). Subsequently, the effect of metformin on primary myotubes was confirmed by culturing primary myoblasts. After differentiation, primary myoblasts from 3-month-old TA muscle and 23-month-old TA muscle were treated with 2 mM metformin using established protocols.[20,21] Metformin was found to increase the expression of myostatin in both young and old primary myotubes (Figure 1H and 1I). For morphological analysis, C2C12 myoblasts were incubated in a differentiation medium for 5 days. siRNA-mediated myostatin knockdown in the background of metformin treatment reduced the atrophy of C2C12 myotubes (Figure 1J). Myotube diameter was calculated (Figure 1K). qRT-PCR was performed to confirm metformin-induced atrophy of C2C12 myotubes. Metformin up-regulates the expression of atrophy-related genes MuRF1 and MAFbx32 (Figure 1L and 1M). To gain insight into the physiological relevance, we used human muscle cells. We investigated the effect of metformin on the mRNA expression of myostatin. Metformin (0.1 and 2 mM) increased the expression of the myostatin dose-dependently (Figure 1N). We investigated the effect of metformin on CK and LDH, indicators of muscle damage. Metformin (0.1 and 2 mM) increased the activity of CK and LDH (Figure 1O and 1P). These results suggest that biguanide drugs, such as metformin, may induce muscle atrophy.

Metformin increased myostatin expression via AMPK

We tested whether the myostatin-upregulating effect of metformin depended on the activation of AMPK, a well-known molecular target of metformin. Evaluation of the AMPK pathway has revealed that several molecules are related to muscle atrophy.[22] Metformin increased the phosphorylation of AMPK at the Thr-172 residue in a dose-dependent and time-dependent manner (Figure 2A and 2B). To elucidate the function of AMPK and the relationship between AMPK and myostatin, we used an AMPK inhibitor (Compound C), siAMPK alpha2, and the CRISPR system. Compound C was able to decrease the expression of myostatin in the background of metformin treatment in C2C12 (Figure 2C). To validate the mechanism underlying metformin-induced muscle atrophy, we performed qRT-PCR and WB using siAMPK alpha2. Similar to Compound C, siAMPK alpha2 decreased myostatin expression in the background of metformin treatment (Figure 2D and 2E). For morphological analysis, C2C12 myoblasts were induced to differentiate by incubating them with the differentiation medium for 5 days. siRNA-mediated
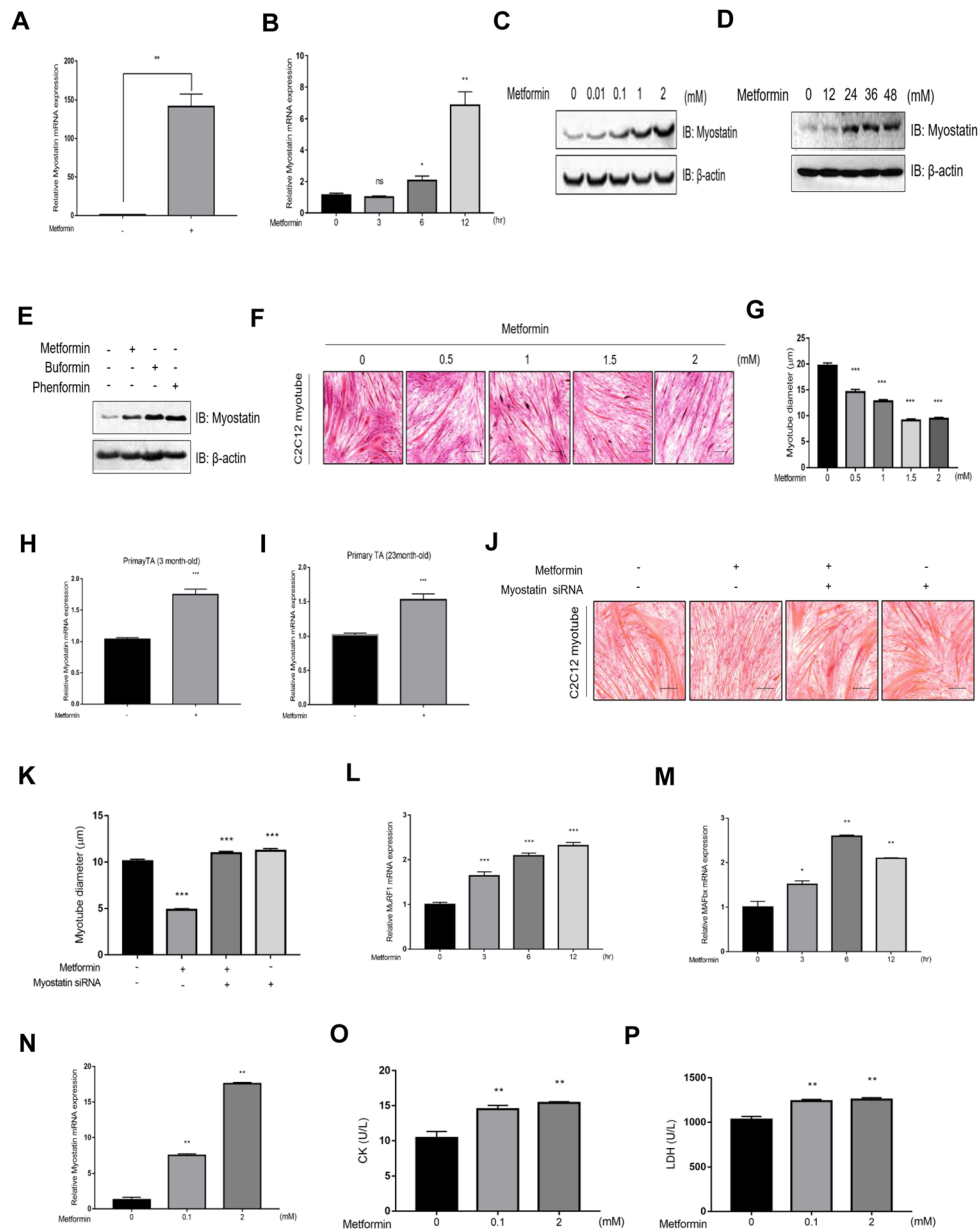
Figure 1 Metformin up-regulates myostatin expression. *(A)* Comparison of the relative mRNA expression of myostatin using real-time PCR (qRT-PCR). C2C12 myotubes were stimulated with metformin (2 mM) for 12 h. *(B)* C2C12 myotubes were stimulated with metformin (2 mM) for the indicated times. PCR was normalized using GAPDH expression. Bars represent the mean ± SEM. *(C)* The expression of myostatin was examined by western blotting (WB). C2C12 myotubes were stimulated for 36 h with indicated concentrations of metformin (0.01–2 mM). Cell lysates were analysed using anti-myostatin and anti-β-actin antibodies. *(D)* C2C12 myotubes were incubated with metformin (2 mM) for the indicated times. Cell lysates were analysed using anti-myostatin and anti-β-actin antibodies. *(E)* The expression of myostatin was evaluated by WB. C2C12 myotubes were stimulated with the biguanides, metformin (2 mM), buformin (50 μM), and phenformin (50 μM) for 24 h. Cell lysates were analysed using anti-myostatin and anti-β-actin antibodies. *(F)* Myotube morphology was examined via haematoxylin and eosin (H&E) staining after metformin treatment (0–2 mM). *(G)* Analysis of the diameter of cultured myotubes. Myotube diameter was calculated using ImageJ. Bars represent the mean ± SEM. *(H, I)* Primary TA myotubes were stimulated with metformin (2 mM) for 24 h. *(J)* C2C12 myotubes were pre-treated with Myostatin siRNA (100 nM) and incubated with metformin (2 mM). Myotube morphology was examined via haematoxylin and eosin (H&E) staining. *(K)* Analysis of the diameter of cultured myotubes. Myotube diameter was calculated using ImageJ. *(L, M)* Comparison of the relative mRNA expression of MuRF1 and MAFbx32 using real-time PCR (qRT-PCR). C2C12 myotubes were stimulated with metformin (2 mM) for the indicated times. PCR was normalized using GAPDH expression. *(N)* Comparison of the relative mRNA expression of myostatin using real-time PCR (qRT-PCR). Human skeletal myoblasts were stimulated with metformin (0.1 and 2 mM) for 12 h. Gene expression was normalized using GAPDH. *(O, P)* Creatine kinase (CK) and lactate dehydrogenase (LDH) activity of human skeletal muscle cells. CK and LDH activity was measured in cytoplasmic extracts and normalized using total protein. Results are expressed as the mean ± SEM. Scale bar, 100 μm. *$P < 0.05$, **$P < 0.01$, ***$P < 0.001$ compared to the control.
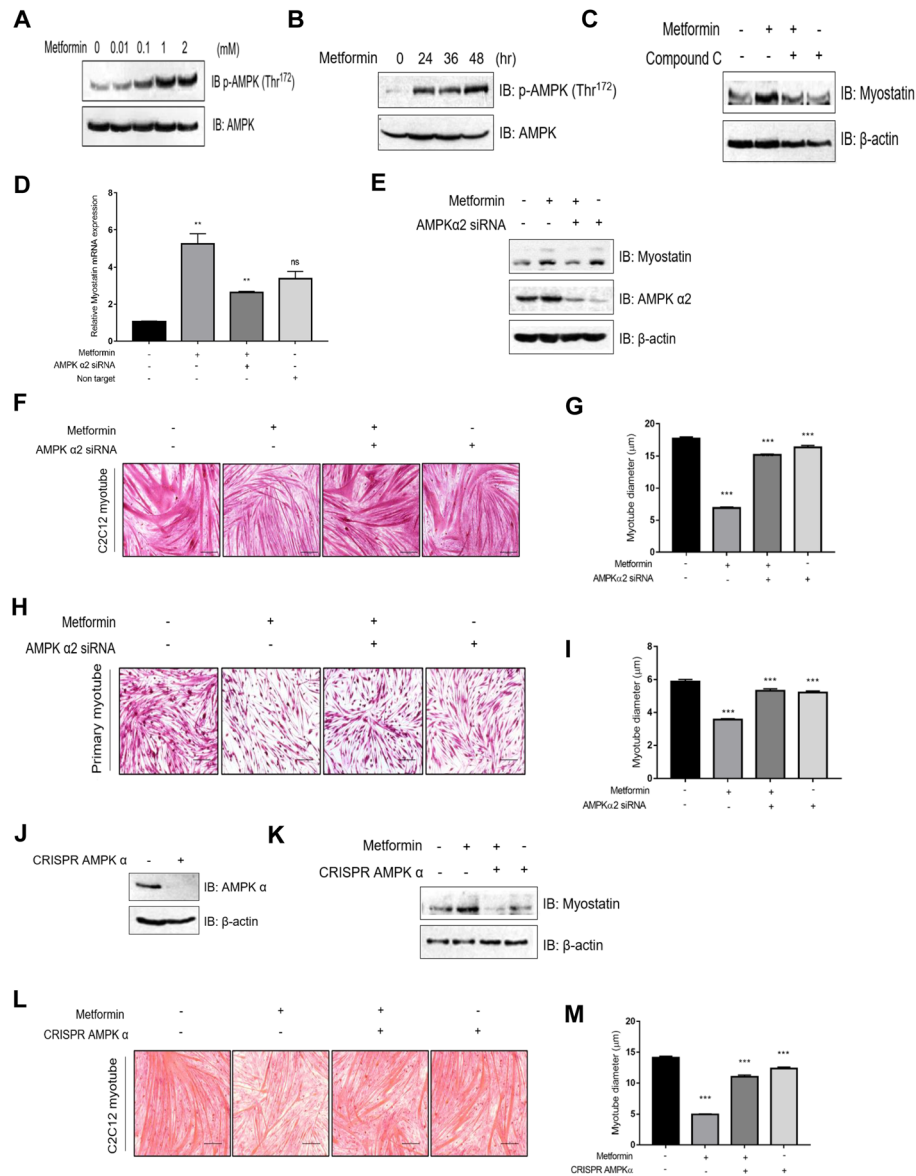
Figure 2 Metformin increases myostatin expression via AMPK. *(A)* The level of p-AMPK was evaluated by western blotting (WB). C2C12 myotubes were stimulated for 36 h with indicated concentrations of metformin (0.01–2 mM). Cell lysates were analysed using anti-phospho-AMPK (Thr[172]) and anti-AMPK antibodies. *(B)* C2C12 myotubes were incubated with metformin (2 mM) for the indicated times. Cell lysates were analysed using anti-phospho-AMPK (Thr[172]), and anti-AMPK antibodies. *(C)* The expression of myostatin was evaluated by WB. C2C12 myotubes were pre-treated with the AMPK inhibitor, Compound C (30 μM), and incubated with metformin (2 mM). Cell lysates were analysed using anti-myostatin and anti-β-actin antibodies. *(D)* Comparison of the relative mRNA expression of myostatin using real-time PCR (qRT-PCR). C2C12 myotubes were pre-treated with AMPK α2 siRNA (100 nM) and incubated with metformin for 24. PCR was normalized using GAPDH. Bars represent the mean ± SEM. *(E)* The expression of myostatin was evaluated by WB analysis. C2C12 myotubes were pre-treated with AMPK α2 siRNA (100 nM) and incubated with metformin (2 mM) for 24 h. Cell lysates were analysed using anti-myostatin, anti-AMPK α2 and anti-β-actin antibodies. *(F)* C2C12 myotubes were pre-treated with AMPK α2 siRNA (100 nM) and incubated with metformin (2 mM). Myotube morphology was examined via haematoxylin and eosin (H&E) staining. *(G)* Analysis of the diameter of cultured myotubes. Myotube diameter was calculated with ImageJ. Bars represent the mean ± SEM. *(H)* Primary TA myotubes were pre-treated with AMPK α2 siRNA and incubated with metformin (2 mM). Myotube morphology was examined via H&E staining. *(I)* Analysis of the diameter of cultured primary myotubes. Primary myotube diameter was calculated with ImageJ. Bars represent the mean ± SEM. *(J)* The expression of AMPK α was evaluated by WB analysis. CRISPR/AMPK α (2 μg) was transfected for 24 h. Cell lysates were analysed using anti-AMPK α, and anti-β-actin antibodies. *(K)* The expression of myostatin was evaluated by WB analysis. C2C12 myotubes were pre-treated with CRISPR/AMPK α and incubated with metformin (2 mM) for 24 h. Cell lysates were analysed using anti-myostatin and anti-β-actin antibodies. *(L)* C2C12 myotubes were pre-treated with CRISPR/AMPK α (2 μg) and incubated with metformin (2 mM). Myotube morphology was examined via haematoxylin and eosin (H&E) staining. *(M)* Analysis of the diameter of cultured myotubes. Myotube diameter was calculated with ImageJ. Results are expressed as the mean ± SEM. Scale bar, 100 μm. **$P < 0.01$, ***$P < 0.001$ compared to the control.

knockdown of AMPK alpha2 reduced the metformin-induced atrophy of C2C12 myotubes (*Figure* 2F). Myotube diameter was calculated (*Figure* 2G). To achieve *ex vivo* conditions, primary myoblasts from mouse TA muscles were induced to differentiate by incubating them with the differentiation medium. The results obtained upon using primary myotubes were similar to those obtained with C2C12 myotubes after siRNA-mediated AMPK knockdown (*Figure* 2H and 2I). Further, CRISPR AMPK alpha was found to decrease myostatin expression following treatment with metformin. Under basal conditions, the levels of total AMPK alpha decreased significantly after AMPK alpha knockdown (*Figure* 2J). Furthermore, CRISPR AMPK alpha in the background of metformin treatment reduced myostatin expression in C2C12 myotubes (*Figure* 2K). For morphological analysis, C2C12 myoblasts were induced to differentiate by incubating them with the differentiation medium for 5 days. Knockdown of AMPK alpha in the background of metformin treatment resulted in reduced atrophy of C2C12 myotubes (*Figure* 2L). Myotube diameter was calculated (*Figure* 2M). Thus, inhibition of AMPK activity might reduce metformin-induced up-regulation of myostatin expression in C2C12 myotubes. These results indicate that metformin impacts the muscle volume via AMPK-dependent myostatin up-regulation.

Metformin-induced up-regulation of myostatin expression in C2C12 myotubes involves FoxO3a

Because AMPK can promote FoxO3a activity by inducing the expression of autophagy-related genes,[23] and the fasting-induction of FoxO3a and MuRF1 requires AMPK,[24] we hypothesized that FoxO3a impacts metformin-induced muscle atrophy by up-regulating myostatin through AMPK. We found that metformin increased FoxO3a expression at mRNA (*Figure* 3A and 3B) and protein levels in a dose-dependent and time-dependent manner (*Figure* 3C and 3D). To confirm the relationship between p-AMPK and FoxO3a, we performed a co-immunoprecipitation assay and found that p-AMPK co-immunoprecipitated with FoxO3A in C2C12 myotubes after 36 h of metformin treatment (*Figure* 3E). To verify the role of FoxO3a in myostatin expression in C2C12 myotubes, we performed qRT-PCR on cells transfected with siFoxO3a. Myostatin expression decreased significantly after siRNA-mediated FoxO3a knockdown (*Figure* 3F). For morphological analysis, the differentiation of C2C12 myoblasts was induced by incubating them with the differentiation medium for 5 days. Knockdown of FoxO3a resulted in the background of metformin treatment reduced the atrophy of C2C12 myotubes (*Figure* 3G). Myotube diameter was calculated (*Figure* 3H). These findings indicate that p-AMPK and FoxO3a are upstream molecules that regulate myostatin expression.

Histone deacetylase 6 is involved in the metformin-mediated regulation of myostatin expression

Previous studies have found that Class IIa HDACs (HDAC4, 5, and 7) recruit HDAC3, thereby causing transcriptional induction via the deacetylation and activation of FOXO family transcription factors[25,26] and that HDAC6 (Class IIb) activates FoxO3a under conditions of denervation muscle atrophy.[27] Based on these results, we hypothesized that metformin might regulate HDAC6 expression, a phenomenon that might result in the activation of FoxO3a. We found that metformin regulates HDAC6 expression in a dose-dependent and time-dependent manner (*Figure* 4A and 4B) and, at a concentration of 2 mM, metformin increases HDAC6 expression at the protein level (*Figure* 4C). Subsequently, we examined whether HDAC6 regulates FoxO3a activity through direct binding. A co-immunoprecipitation assay revealed that HDAC6 binds to FoxO3a after metformin treatment (*Figure* 4D). To confirm that HDAC6 is associated with AMPK, we transfected cells with siAMPK alpha2 and measured the transcript-level expression of HDAC6, which increased after metformin treatment and decreased after treatment with siAMPK alpha2 (*Figure* 4E). Protein levels were correlated with the mRNA levels (*Figure* 4F). Consistent with the results of siRNA-mediated AMPK alpha2 knockdown, transfection with CRISPR AMPK alpha resulted in decreased expression of HDAC6 (*Figure* 4G). After inhibiting HDAC6 from metformin-treated C2C12 myotubes, myostatin expression level also decreased (*Figure* 4H and 4I). For morphological analysis, the differentiation of C2C12 myoblasts was induced by incubating them with the differentiation medium for 5 days. siRNA-mediated knockdown of HDAC6 in the background of metformin treatment reduced the atrophy of C2C12 myotubes (*Figure* 4J). Myotube diameter was calculated (*Figure* 4K). These findings suggest that HDAC6 is a key molecule for the regulation of myostatin expression and that AMPK is a key upstream molecule of HDAC6.

FoxO3a regulates myostatin expression by binding to its promoter region

To determine whether metformin regulates myostatin through transcriptional regulation, we used luciferase reporter constructs containing the myostatin promoter. We found that metformin induced the activity of the myostatin promoter reporter, which contained fragments from −400 to +200 bp. Luciferase activity was normalized against a β-galactosidase reporter plasmid, and the results are presented relative to the activity of the empty pGL4.15. After transfection, C2C12 myotubes were treated with metformin for 12 h. Metformin treatment enhanced the activity of the myostatin promoter (*Figure* 5A). We hypothesized that
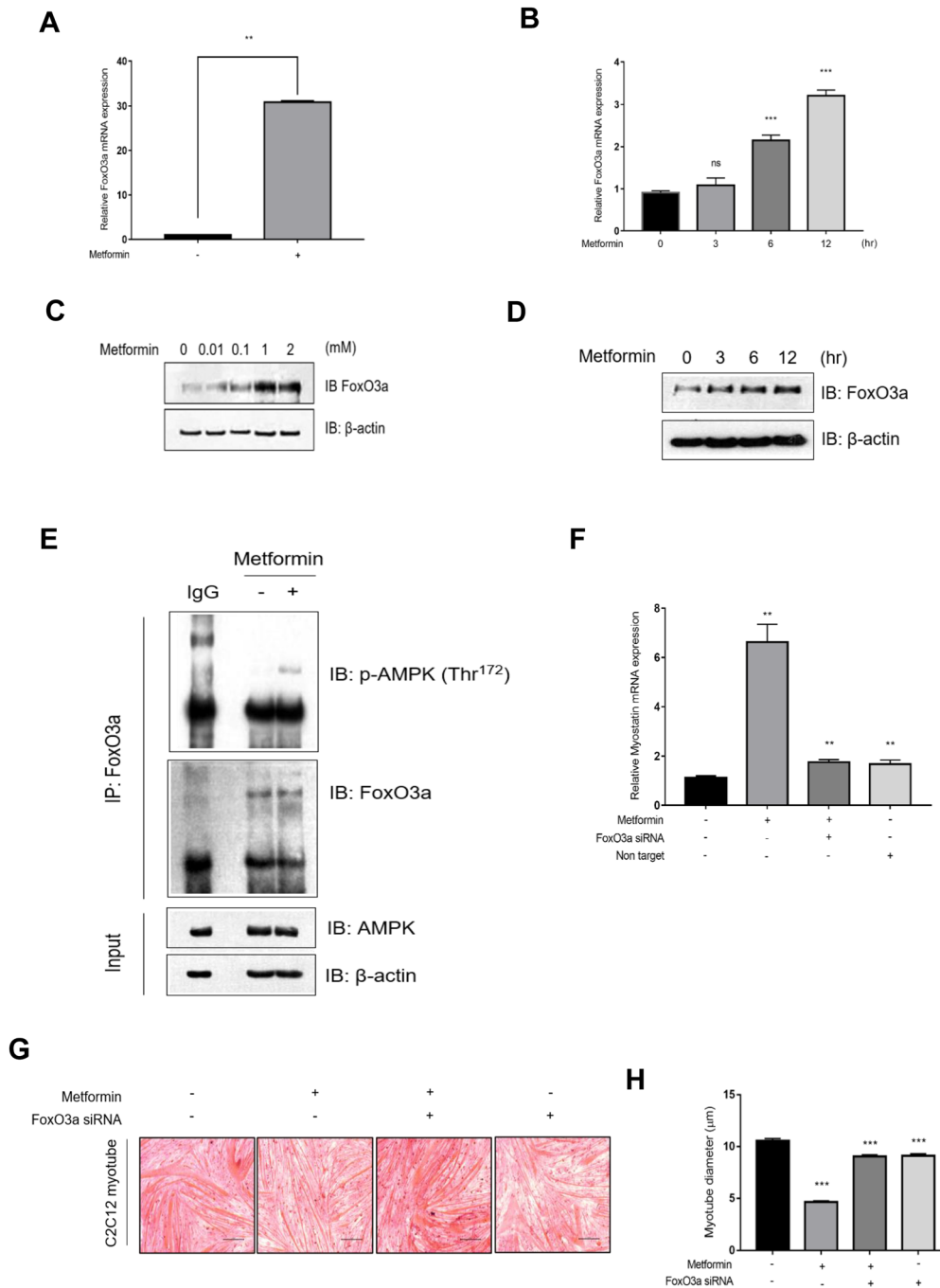
Figure 3 Metformin regulates myostatin, via FoxO3a. *(A)* Comparison of the relative FoxO3a mRNA expression using real-time PCR (qRT-PCR). C2C12 myotubes were stimulated with metformin (2 mM) for 12 h. *(B)* C2C12 myotubes were stimulated with metformin (2 mM) for the indicated times. PCR was normalized using GAPDH. The bars represent the mean ± SEM. *(C)* The expression of FoxO3a was evaluated by western blotting (WB). C2C12 myotubes were stimulated for 36 h with indicated concentrations of metformin (0.01–2 mM). Cell lysates were analysed using anti-FoxO3a and anti-β-actin antibodies. *(D)* The expression of FoxO3a was evaluated by WB. C2C12 myotubes were stimulated with metformin (2 mM) for the indicated times. Cell lysates were analysed using anti-FoxO3a and anti-β-actin antibodies. *(E)* A co-immunoprecipitation assay used lysate from metformin- (2 mM, 36 h) treated C2C12 myotubes. Immunoprecipitations was performed with the anti-FoxO3a antibody. Cell lysates were analysed using anti-IgG, anti-FoxO3a, anti-p-AMPK (Thr^{172}), anti-AMPK, and anti-β-actin antibodies. IgG was used as the negative control. *(F)* Comparison of the relative mRNA expression of myostatin using real-time PCR (qRT-PCR). C2C12 myotubes were pre-treated with FoxO3a siRNA (100 nM) and incubated with metformin for 24 h. PCR was normalized using GAPDH. *(G)* C2C12 myotubes were pre-treated with FoxO3a siRNA (100 nM) and incubated with metformin (2 mM). Myotube morphology was examined via haematoxylin and eosin (H&E) staining. *(H)* Analysis of the diameter of cultured myotubes. Myotube diameter was calculated with ImageJ. Results are expressed as the mean ± SEM. Scale bar, 100 μm. **$P < 0.01$, ***$P < 0.001$ compared to the control.
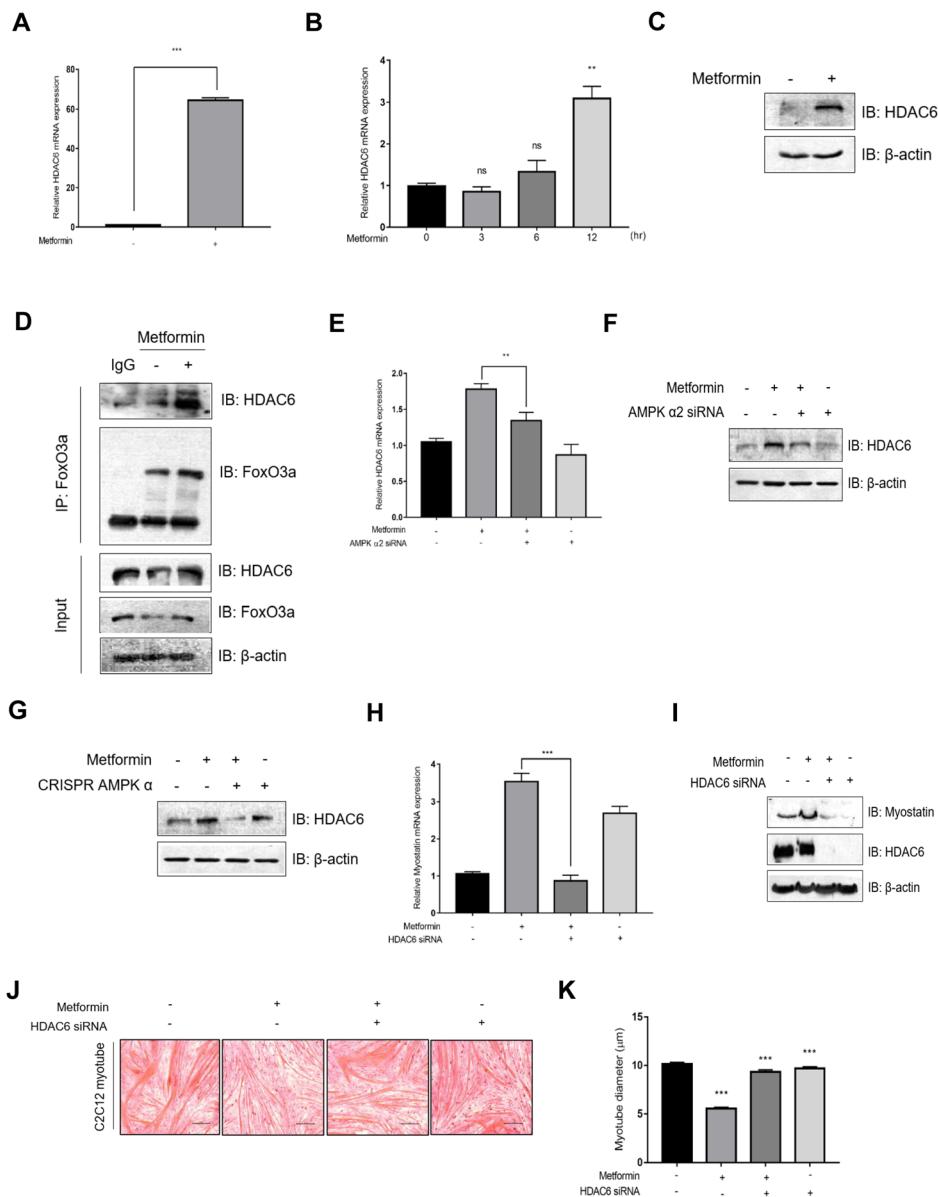
Figure 4 HDAC6 is involved in the up-regulation of myostatin. *(A)* Comparison of the relative HDAC6 mRNA expression using real-time PCR (qRT-PCR). C2C12 myotubes were stimulated with metformin (2 mM) for 12 h. *(B)* C2C12 myotubes were stimulated with metformin (2 mM) for the indicated times. PCR was normalized using GAPDH expression. Bars represent the mean ± SEM. *(C)* HDAC6 expression was evaluated by western blotting (WB). C2C12 myotubes were stimulated with metformin (2 mM) for 24 h. Cell lysates were immunoblotted using anti-HDAC6 and anti-β-actin antibodies. *(D)* A co-immunoprecipitation assay used lysates from metformin-treated (2 mM, 36 h) C2C12 myotubes. Immunoprecipitation was performed with the anti-FoxO3a antibody. Cell lysates were immunoblotted using anti-IgG, anti-FoxO3a, anti HDAC6, and anti-β-actin antibodies. IgG was used as a negative control. *(E)* Comparison of the relative HDAC6 mRNA expression using real-time PCR (qRT-PCR). C2C12 myotubes were pre-treated with AMPK α2 siRNA (100 nM) and incubated with metformin for 24 h. PCR was normalized using GAPDH expression. Bars represent mean ± SEM. *(F)* The expression of HDAC6 was evaluated by western blotting (WB). C2C12 myotubes were pre-treated with AMPK α2 siRNA (100 nM), incubated with metformin (2 mM) for 24 h, and analysed by WB analysis. Cell lysates were analysed using anti-HDAC6 and anti-β-actin antibodies. *(G)* C2C12 myotubes were pre-treated with CRISPR/AMPK α sgRNA (2 μg), incubated with metformin (2 mM) for 24 h, and analysed by WB analysis. Cell lysates were immunoblotted using anti-HDAC6 and anti-β-actin antibodies. *(H)* Comparison of the relative mRNA expression of myostatin using real-time PCR (qRT-PCR). C2C12 myotubes were pre-treated with HDAC6 siRNA (100 nM) and incubated with metformin for 24 h. PCR was normalized using GAPDH expression. Bars represent the mean ± SEM. *(I)* C2C12 myotubes were pre-treated with HDAC6 siRNA, incubated with metformin (2 mM) for 24 h, and analysed by WB analysis. Cell lysates were immunoblotted using anti-myostatin, anti-HDAC6, and anti-β-actin antibodies. *(J)* C2C12 myotubes were pre-treated with HDAC6 siRNA (100 nM) and incubated with metformin (2 mM). Myotube morphology was examined via haematoxylin and eosin (H&E) staining. *(K)* Analysis of the diameter of cultured myotubes. Myotube diameter was calculated with ImageJ. Results are expressed as the mean ± SEM. Scale bar, 100 μm. Results are expressed as the mean ± SEM. **$P < 0.01$, ***$P < 0.001$ compared to the control.
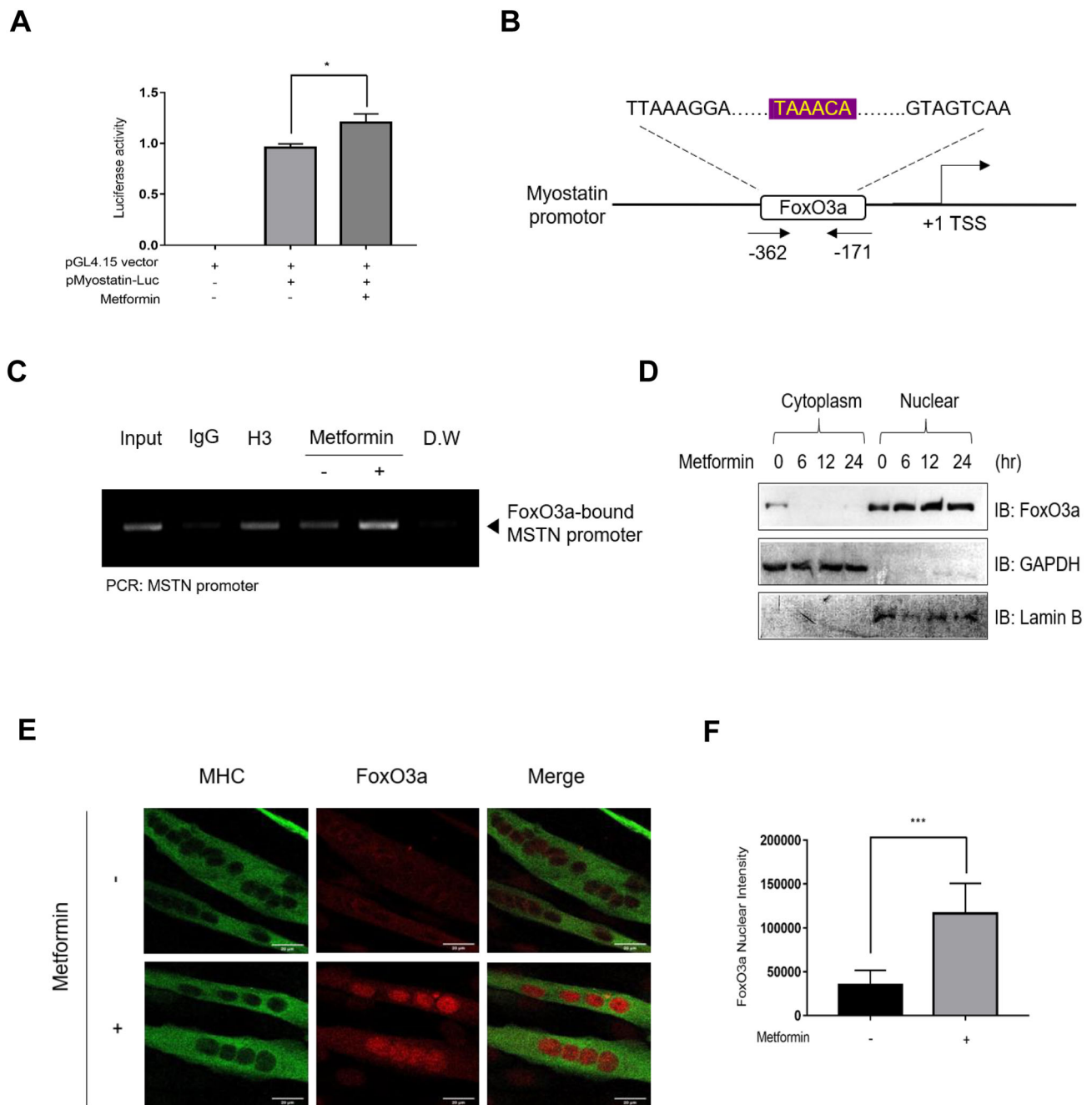
Figure 5 FoxO3a regulates myostatin by binding to its promotor region via subcellular localization. *(A)* Cells were transfected with the p-myostatin-Luc firefly luciferase reporter plasmid (1 μg) and β-galactosidase control reporter plasmid (100 ng). The next day, metformin was administered for 12 h. The cell extracts were analysed using a Promega luciferase assay kit. The graphs display the mean ratios of the firefly reporter and β-galactosidase control. Bars represent the mean ± SEM. *(B)* Framework of the mouse myostatin gene. The arrows indicate the location of putative FoxO3a binding site in the myostatin promotor region. *(C)* ChIP experiments were performed using digested chromatin from C2C12 myotubes. Purified DNAs were analysed by standard PCR methods using ChIP myostatin primers. *(D)* Subcellular localization of FoxO3. The C2C12 myotubes were fractionated into nuclear and cytoplasmic fractions after metformin treatment for the indicated times. The fractions were immunoblotted to detect anti-FoxO3a, cytosolic protein anti-GAPDH, nuclear proteins, anti-lamin B antibodies. *(E)* C2C12 myoblasts treated with metformin were subjected to immunofluorescence (IF) analysis with anti-MHC (green), anti-FoxO3a (red), and confocal microscopy. *(F)* Results of immunofluorescence (IF) nuclear intensity quantification, expressed as the mean ± SEM. Scale bar, 20 μm. *$P < 0.05$, ***$P < 0.001$ compared to the control.

metformin directly regulates myostatin via FoxO3a. Forkhead transcription factor families contain similar DNA-binding domains.[28,29] We predicted putative FoxO3a-binding sites (−362 and −172) in the myostatin promoter (*Figure* 5B). ChIP experiments revealed that FoxO3a binds to the putative binding site in the myostatin promoter in C2C12 cells (*Figure* 5C). To determine whether metformin promoted the subcellular localization of FoxO3a, we performed cytoplasmic-nuclear fractionation. Interestingly, metformin treatment induced the nuclear localization of FoxO3a (*Figure* 5D). Confocal microscopy revealed that the expression of FoxO3a increased in the nucleus after metformin treatment (*Figure* 5E). FoxO3a significantly increased the nuclear intensity of FoxO3a after metformin treatment (*Figure* 5F). These results indicate that metformin induces the direct binding between FoxO3a and the myostatin promoter.

Metformin's effects on the muscles of db/db mice

Patients with T2DM exhibit a significant decline in muscle mass, strength, and function.[30] Accordingly, an imbalance in the synthesis and degradation of contractile proteins can occur in these patients. Systemic inflammation initiated by obesity and insulin resistance promotes muscle atrophy in patients with T2DM.[31] Therefore, before evaluating our findings in an *in vivo* model of diabetes, we sought to determine the muscle-wasting effects of metformin in an *in vitro* model of insulin-resistant T2DM. We established an insulin-resistant model in C2C12 cells in which insulin resistance responses were exhibited after insulin treatment using high concentration of insulin and TNF-α, in accordance with established protocols.[32] As expected, a decrease in the phosphorylation of Akt at serine 473 was observed (*Figure* 6A). To confirm the myostatin-regulatory effects of metformin in insulin-resistant conditions, we verified the transcript-level expression of myostatin after metformin treatment. A greater increase in myostatin mRNA was observed in groups treated with insulin, TNF-α, and metformin than that in the group treated with metformin alone (*Figure* 6B), indicating that metformin could impair muscle function in an insulin-resistant state. To confirm the blood glucose-reducing effect of metformin, we measured the blood glucose levels in animals. Metformin-treated db/db mice showed lower blood glucose levels than control animals (*Figure* 6C). To evaluate the effect of metformin on the cross-sectional area of muscle fibres, we conducted H&E staining of GC muscles and estimated the fibre size. Our data showed the distribution of myofibre size in each group. Metformin-treated db/db mice had a leftward shift in the distribution of fibre sizes compared with the controls (*Figure* 6D). The average fibre cross-sectional area in the GC muscles was quantified by H&E staining (*Figure* 6E). Next, we confirmed the expression of myostatin mRNA in the hindlimb

muscles. Myostatin levels increased in metformin-treated GC muscles (*Figure* 6F). However, other muscles such as the TA, quadriceps (QC), and extensor digitorum longus (EDL) did not exhibit any significant differences between the metformin-treated group and the control group (*Figure* 6G, 6H, and 6I). The grip strength test also did not reveal any differences between the control and metformin-treated db/db mice (*Figure* 6J). ELISA did not reveal a significant difference in the serum myoglobin levels in metformin-treated db/db mice (compared to control mice) (*Figure* 6K). These results demonstrate that metformin impairs muscle function but has negligible effects in db/db mice. This suggests that metformin can affect the muscle via complicated mechanisms.

The effect of metformin in wild-type mice

Metformin does not provide benefits for muscle function, but its negative effects on muscle are minimal in db/db mice. We conducted the same experiments in wild-type mice to verify the effects of metformin on muscle atrophy. Similar to the results in the db/db mice, the cross-sectional area of muscle fibres in the GC muscle showed a leftward shift in the distribution of myofibre sizes in metformin-treated wild-type mice (compared with the controls) (*Figure* 7A). The average fibre cross-sectional area in the GC muscles was quantified by H&E staining (*Figure* 7B). Myostatin levels increased significantly in the GC muscles of metformin-treated wild-type mice compared to those in the controls (*Figure* 7C). However, as confirmed in the db/db mice, TA, QC, and EDL muscles did not differ significantly between the metformin-treated mice and the controls (*Figure* 7D, 7E, and 7F). In contrast to that of the db/db mice, the grip strength of the wild-type mice treated with metformin was significantly lower than that of the control group (*Figure* 7G). Moreover, the serum myoglobin level in metformin-treated wild-type mice was significantly lower than that in the controls (*Figure* 7H). These results indicate that metformin negatively affects muscle function, and the effects are greater in wild-type mice than those in the db/db mice.

Discussion

Our findings reveal the role of metformin in the regulation of muscle wasting at the transcriptional level. Although first-line biguanide metformin is often administered to patients with T2DM, its long-term administration can cause several side effects, including those that affect muscle function. Currently, the effect of metformin on the muscles is controversial. Blood glucose levels and other conditions can also induce muscle atrophy. Metformin is known to produce a glucose-lowering effect that is accompanied by improvements in insulin sensitivity; however, it is also known to in-
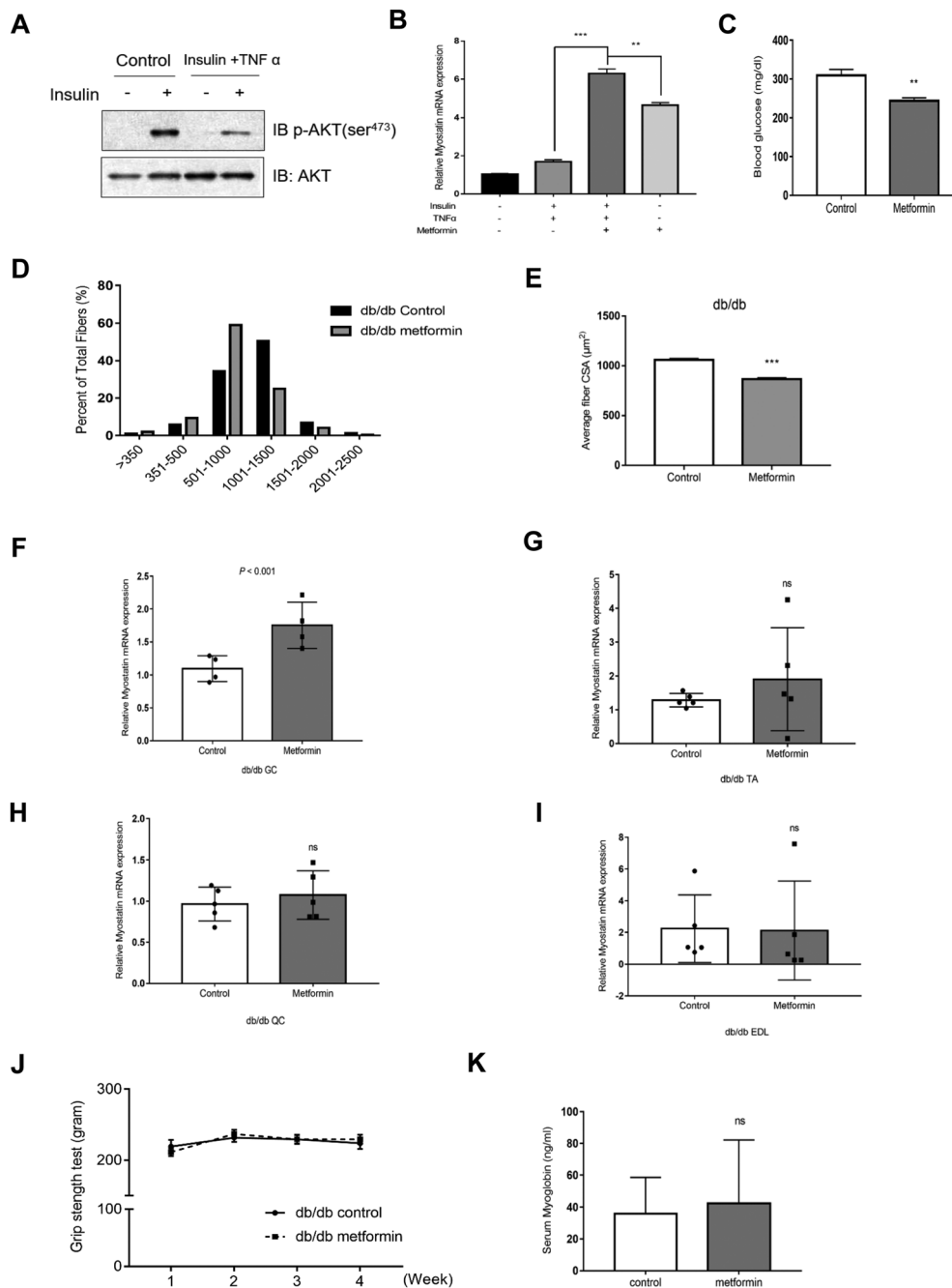
Figure 6 Reduced muscle atrophy effects of metformin in db/db mice. *(A)* The expression of p-AKT (ser^{473}) was determined via western blotting (WB) analysis. C2C12 myotubes were pre-treated with insulin (100 nM) and TNF-α (2.5 nM) for 24 h, and then stimulated with insulin (100 nM) for 15 min. Cell lysates were analysed using anti-phospho-AKT (ser^{473}), and anti-AKT antibodies. *(B)* Comparison of the relative mRNA expression of myostatin using real-time PCR (qRT-PCR). C2C12 myotubes were pre-treated with insulin (100 nM) and TNF-α (2.5 nM) for 24 h, and then incubated with metformin for 24 h. PCR was normalized using GAPDH. The bars represent the mean ± SEM. *(C)* Blood glucose level (mg/dL) in metformin-treated db/db mice, measured after overnight fasting. Bars represent the mean ± SEM. *(D)* Muscle fibre cross-sectional area in the GC muscles of db/db mice. Data show the fibre size distribution. *(E)* Average fibre cross-sectional area (CSA) of GC muscles. Bars represent the mean ± SEM. *(F-I)* Real-time PCR (qRT-PCR) comparison of the relative mRNA expression of myostatin in GC, TA, QC, and EDL muscles obtained from control and metformin- (250 mg/kg) treated db/db mice. Only the GC samples showed significantly increased myostatin expression. PCR was normalized using GAPDH. Bars represent the mean ± SEM. *(J)* Grip strength test; fore and hindlimb (four paws) grip force measurements. Tests were performed weekly and averaged across three trials. Data are expressed as the mean ± SEM. *n* = 10/group. *(K)* Enzyme-linked immunosorbent assay (ELISA). Data indicate the serum myoglobin level (ng/mL). The serum myoglobin levels of the db/db mice showed no significant change from the controls. Results are expressed as the mean ± SEM. **$P < 0.01$, ***$P < 0.001$ compared to the control.
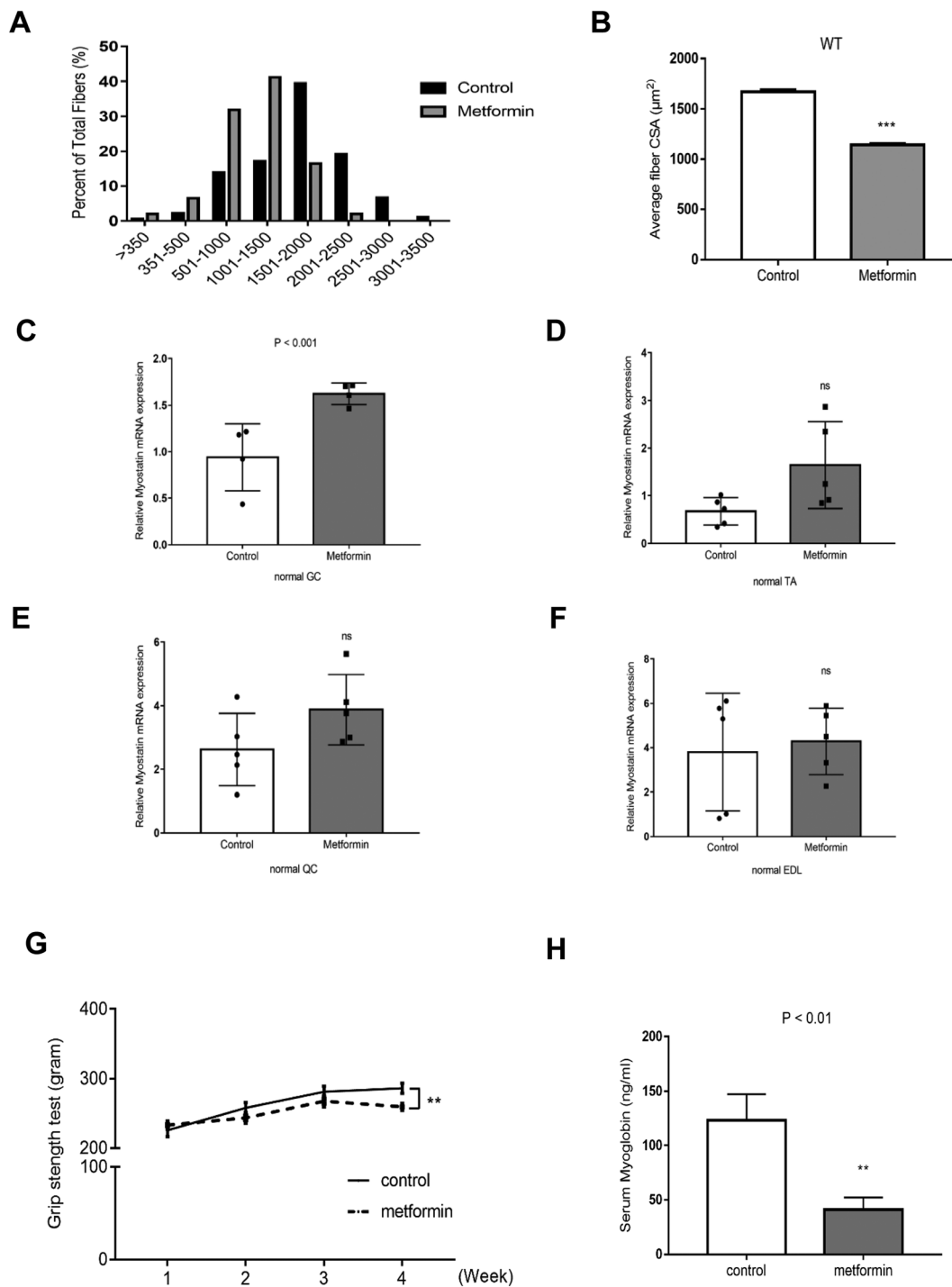
Figure 7 Metformin negatively affects muscle function in wild-type mice. *(A)* Data indicate the muscle fibre cross-sectional area of the GC muscle wild-type mice. Data show the fibre size distribution. *(B)* Average fibre cross-sectional area (CSA) of GC muscles. Bars represent the mean ± SEM. *(C–F)* Real-time PCR (qRT-PCR) comparison of the relative mRNA expression of myostatin in the GC, TA, QC and EDL muscles of control and metformin-treated wild-type mice. Only the GC muscle showed significantly increased myostatin expression. PCR was normalized using GAPDH. The bars represent the mean ± SEM. *(G)* Grip strength test; fore-/hindlimb (four paws) grip force measurements. Tests were performed weekly and averaged across three trials. The metformin-treated wild-type mice showed decreased muscle grip strength. Data are expressed as the mean ± SEM. *n* = 10/group. *(H)* Enzyme-linked immunosorbent assay (ELISA). Data indicate the serum myoglobin level (ng/mL). The serum myoglobin levels of the wild-type mice decreased significantly compared with the controls. Results are expressed as the mean ± SEM. **$P < 0.01$, ***$P < 0.001$ compared to the control.

crease the levels of p-AMPK and myostatin, a muscle atrophy-related molecule. Thus, three different arguments arise. A recent study revealed that metformin negatively affects the hypertrophic response to resistance training in healthy older individuals. Because metformin reduces inflammation, the researcher of the study hypothesized that metformin would augment the muscle response; however, the placebo group had more gains in lean body and thigh muscle mass than the metformin-treated group.[33] Another study suggested that leg lean mass and appendicular skeletal muscle mass were significantly lower in older men with T2DM than in controls. Notably, 87% of patients in the T2DM group received metformin.[30] However, previous investigations have indicated that metformin-receiving diabetes mellitus group showed an increase in appendicular lean mass. These data suggest that the use of insulin sensitizers, particularly metformin, could attenuate the loss of appendicular lean mass in older men with diabetes. Another study found that 5-aminoimidazole-4-carboxamide ribonucleotide (AICAR), metformin, and IFN/TNF treatments all activated AMPK, but only AICAR prevented IFN/TNF-induced atrophy. These results clearly demonstrate that both AICAR and metformin activate AMPK, but co-treatment with AICAR, excluding metformin, prevents the progression of cytokine-induced myotube wasting.[34] On the other hand, our results support the negative effects of metformin on muscle hypertrophy. Furthermore, our in vivo findings from GC muscles after metformin treatment correlated with our in vitro findings. However, other hindlimb muscles, TA, QC, and EDL did not show significant changes in myostatin expression in wild-type and db/db mice. In addition, the effect of metformin on muscle mass also differed depending on the muscle type. The weight of QC and soleus decreased, but other muscles, such as EDL, GC, and TA, showed no significant changes. These results suggest that there might be a mechanism regulating muscle mass other than myostatin. Importantly, our results showed significant differences in the response to metformin in diabetic and non-diabetic conditions. First, db/db mice administered metformin did not differ significantly from the control group in the grip strength test, but the wild-type mice administered metformin had a significant decrease in muscle grip strength. Second, the myoglobin level of metformin-treated wild-type mice decreased in the serum analysis. Therefore, metformin has a complicated effect on the muscle regulation mechanisms. In db/db mice, the glucose-lowering effect of metformin may partially offset its muscle-wasting effect.

Accordingly, whether metformin induces muscle wasting in humans with T2DM remains unknown. Based on our in vitro results, the up-regulation of myostatin in response to metformin is controlled by activated p-AMPK, which regulates subcellular localization and ultimately enables binding between FoxO3a and myostatin. In the myostatin promoter region, FoxO3a binds to the putative binding site of myostatin by directly activating its expression. Therefore, it can cause muscle wasting. Because HDAC6 also binds to FoxO3a in this molecular process, we hypothesized that HDAC6-mediated myostatin up-regulation might be related to its deacetylation activity. In other words, HDAC6 might regulate acetylated FoxO3a and increase FoxO3a expression. HDAC6 may also regulate muscle atrophy. This study is the first to provide a clear molecular mechanism for the effect of metformin on muscle function. Moreover, we identified the novel muscle atrophy effects of the AMPK- and HDAC6-FoxO3a-myostatin axis at the transcriptional level. We also identified that the transcriptional and epigenetic pathways induced by metformin could cause muscle wasting and induce negative effects in T2DM patients treated with metformin. To date, a broad range of metformin has been used in experiments.[35] In vitro studies and in vivo used much higher doses of metformin than those clinical studies.[16,36,37] In the present study, we used 2 mM in vitro and 250 mg/kg in vivo. These doses are slightly higher than the therapeutic concentrations of metformin in patients, but within the ranges of other studies used metformin. In the future, more studies are necessary to define the relationship between dose-dependent efficacy and the corresponding plasma concentration of metformin.

Conflicts of interest

All authors declare that they have no conflicts of interest.

Ethical guidelines

The authors of this manuscript certify that they complied with the ethical guidelines for authorship and publishing of the Journal of Cachexia, Sarcopenia, and Muscle.[38]

References

1. Schiaffino S, Dyar KA, Ciciliot S, Blaauw B, Sandri M. Mechanisms regulating skeletal muscle growth and atrophy. *FEBS J* 2013;**280**:4294–4314.
2. Bonaldo P, Sandri M. Cellular and molecular mechanisms of muscle atrophy. *Dis Model Mech* 2013;**6**:25–39.
3. Fanzani A, Conraads VM, Penna F, Martinet W. Molecular and cellular mechanisms of skeletal muscle atrophy: an update. *J Cachexia Sarcopenia Muscle* 2012;**3**:163–179.
4. Manfredi LH, Paula-Gomes S, Zanon NM, Kettelhut IC. Myostatin promotes distinct responses on protein metabolism of skeletal and cardiac muscle fibers of rodents. *Braz J Med Biol Res* 2017;**50**:e6733.
5. Hoogaars WMH, Jaspers RT. Past, present, and future perspective of targeting myostatin and related signaling pathways to counteract muscle atrophy. *Adv Exp Med Biol* 2018;**1088**:153–206.
6. Rodriguez J, Vernus B, Chelh I, Cassar-Malek I, Gabillard JC, Hadj Sassi A, et al. Myostatin and the skeletal muscle atrophy and hypertrophy signaling pathways. *Cell Mol Life Sci* 2014;**71**:4361–4371.
7. Latres E, Pangilinan J, Miloscio L, Bauerlein R, Na E, Potocky TB, et al. Myostatin blockade with a fully human monoclonal antibody induces muscle hypertrophy and reverses muscle atrophy in young and aged mice. *Skelet Muscle* 2015;**5**:34.
8. St. Andre M, Johnson M, Bansal PN, Wellen J, Robertson A, Opsahl A, et al. A mouse anti-myostatin antibody increases muscle mass and improves muscle strength and contractility in the mdx mouse model of Duchenne muscular dystrophy and its humanized equivalent, domagrozumab (PF-06252616), increases muscle volume in cynomolgus monkeys. *Skelet Muscle* 2017;**7**:25.
9. Mesinovic J, Zengin A, De Courten B, Ebeling PR, Scott D. Sarcopenia and type 2 diabetes mellitus: a bidirectional relationship. *Diab Metab Syndr Obes* 2019;**12**:1057–1072.
10. Guerrero N, Bunout D, Hirsch S, Barrera G, Leiva L, Henríquez S, et al. Premature loss of muscle mass and function in type 2 diabetes. *Diabetes Res Clin Pract* 2016;**117**:32–38.
11. Wang X, Hu Z, Hu J, Du J, Mitch WE. Insulin resistance accelerates muscle protein degradation: activation of the ubiquitin-proteasome pathway by defects in muscle cell signaling. *Endocrinology* 2006;**147**:4160–4168.
12. Thomson DM. The role of AMPK in the regulation of skeletal muscle size, hypertrophy, and regeneration. *Int J Mol Sci* 2018;**19**.
13. Nakashima K, Yakabe Y. AMPK activation stimulates myofibrillar protein degradation and expression of atrophy-related ubiquitin ligases by increasing FOXO transcription factors in C2C12 myotubes. *Biosci Biotechnol Biochem* 2007;**71**:1650–1656.

14. Madsen KS, Chi Y, Metzendorf MI, Richter B, Hemmingsen B. Metformin for prevention or delay of type 2 diabetes mellitus and its associated complications in persons at increased risk for the development of type 2 diabetes mellitus. *Cochrane Database Syst Rev* 2019;**12**:CD008558.
15. Sanchez-Rangel E, Inzucchi SE. Metformin: clinical use in type 2 diabetes. *Diabetologia* 2017;**60**:1586–1593.
16. Das AK, Yang QY, Fu X, Liang JF, Duarte MS, Zhu MJ, et al. AMP-activated protein kinase stimulates myostatin expression in C2C12 cells. *Biochem Biophys Res Commun* 2012;**427**:36–40.
17. De Lima EA, de Sousa LGO, Teixeira AA, Marshall AG, Zanchi NE, Neto JCR. Aerobic exercise, but not metformin, prevents reduction of muscular performance by AMPk activation in mice on doxorubicin chemotherapy. *J Cell Physiol* 2018;**233**:9652–9662.
18. de Fatima Silva F, Ortiz-Silva M, Galia WBS, Cassolla P, da Silva FG, Graciano MFR, et al. Effects of metformin on insulin resistance and metabolic disorders in tumor-bearing rats with advanced cachexia. *Can J Physiol Pharmacol* 2018;**96**:498–505.
19. Krawiec BJ, Nystrom GJ, Frost RA, Jefferson LS, Lang CH. AMP-activated protein kinase agonists increase mRNA content of the muscle-specific ubiquitin ligases MAFbx and MuRF1 in C2C12 cells. *Am J Physiol Endocrinol Metab* 2007;**292**:E1555–E1567.
20. Springer ML, Rando TA, Blau HM. Gene delivery to muscle. *Curr Protoc Hum Genet* 2001;**31**:13.14. 11–13.14. 19.
21. Bois PR, Grosveld GC. FKHR (FOXO1a) is required for myotube fusion of primary mouse myoblasts. *EMBO J* 2003;**22**:1147–1157.
22. Guo Y, Meng J, Tang Y, Wang T, Wei B, Feng R, et al. AMP-activated kinase α2 deficiency protects mice from denervation-induced skeletal muscle atrophy. *Arch Biochem Biophys* 2016;**600**:56–60.
23. Sanchez AM, Csibi A, Raibon A, Cornille K, Gay S, Bernardi H, et al. AMPK promotes skeletal muscle autophagy through activation of forkhead FoxO3a and interaction with Ulk1. *J Cell Biochem* 2012;**113**:695–710.
24. Fix DK, Counts BR, Smuder AJ, Sarzynski MA, Koh HJ, Carson JA. Wheel running improves fasting-induced AMPK signaling in skeletal muscle from tumor-bearing mice. *Physiol Rep* 2021;**9**:e14924.
25. Mihaylova MM, Vasquez DS, Ravnskjaer K, Denechaud PD, Yu RT, Alvarez JG, et al. Class IIa histone deacetylases are hormone-activated regulators of FOXO and mammalian glucose homeostasis. *Cell* 2011;**145**:607–621.
26. Fang M, Fan Z, Tian W, Zhao Y, Li P, Xu H, et al. HDAC4 mediates IFN-γ induced disruption of energy expenditure-related gene expression by repressing SIRT1 tran-

scription in skeletal muscle cells. *Biochim Biophys Acta* 1859;**2016**:294–305.
27. Ratti F, Ramond F, Moncollin V, Simonet T, Milan G, Méjat A, et al. Histone deacetylase 6 is a FoxO transcription factor-dependent effector in skeletal muscle atrophy. *J Biol Chem* 2015;**290**:4215–4224.
28. Chen X, Ji Z, Webber A, Sharrocks AD. Genome-wide binding studies reveal DNA binding specificity mechanisms and functional interplay amongst Forkhead transcription factors. *Nucleic Acids Res* 2016;**44**:1566–1578.
29. Brian C, Jackson CC, Daniel W. Nebert and Vasilis Vasiliou. Update of human and mouse forkhead box (FOX) gene families. *Hum Genomics Proteomics* 2010;**4**:345–352.
30. Leenders M, Verdijk LB, van der Hoeven L, Adam JJ, van Kranenburg J, Nilwik R, et al. Patients with type 2 diabetes show a greater decline in muscle mass, muscle strength, and functional capacity with aging. *J Am Med Dir Assoc* 2013;**14**:585–592.
31. Perry BD, Caldow MK, Brennan-Speranza TC, Sbaraglia M, Jerums G, Garnham A, et al. Muscle atrophy in patients with type 2 diabetes mellitus: roles of inflammatory pathways, physical activity and exercise. *Exerc Immunol Rev* 2016;**22**:94–108.
32. Lo KA, Labadorf A, Kennedy NJ, Han MS, Yap YS, Matthews B, et al. Analysis of in vitro insulin-resistance models and their physiological relevance to in vivo diet-induced adipose insulin resistance. *Cell Rep* 2013;**5**:259–270.
33. Walton RG, Dungan CM, Long DE, Tuggle SC, Kosmac K, Peck BD, et al. Metformin blunts muscle hypertrophy in response to progressive resistance exercise training in older adults: a randomized, double-blind, placebo-controlled, multicenter trial: the MASTERS trial. *Aging Cell* 2019;**18**:e13039.
34. Hall DT, Griss T, Ma JF, Sanchez BJ, Sadek J, Tremblay AMK, et al. The AMPK agonist 5-aminoimidazole-4-carboxamide ribonucleotide (AICAR), but not metformin, prevents inflammation-associated cachectic muscle wasting. *EMBO Mol Med* 2018;**10**:e8307.
35. Kajbaf F, De Broe ME, Lalau J-D. Therapeutic concentrations of metformin: a systematic review. *Clin Pharmacokinet* 2016;**55**:439–459.
36. Kalender A, Selvaraj A, Kim SY, Gulati P, Brule S, Viollet B, et al. Metformin, independent of AMPK, inhibits mTORC1 in a rag GTPase-dependent manner. *Cell Metab* 2010;**11**:390–401.
37. Rivera ME, Lyon ES, Vaughan RA. Effect of metformin on myotube BCAA catabolism. *J Cell Biochem* 2020;**121**:816–827.
38. von Haehling S, Morley JE, Coats AJS, Anker SD. Ethical guidelines for publishing in the Journal of Cachexia, Sarcopenia and Muscle: update 2019. *J Cachexia Sarcopenia Muscle* 2019;**10**:1143–1145.